PROCEEDINGS OF SCIENCE

Analytic Continuation of the Quark Density in Lattice QC_2D with respect to Quark Chemical Potential

A. M. Begun,[a] **V. G. Bornyakov,**[a,b,c] **N. V. Gerasimeniuk,**[c] **V. A. Goy,**[a,d] **A. Nakamura,**[a,e] **R. N. Rogalyov**[b,*] **and V. Vovchenko**[f]

[a] *Pacific Quantum Center, Far Eastern Federal University, 690950 Vladivostok, Russia*

[b] *Institute for High Energy Physics of the NRC "Kurchatov Institute", 142281 Protvino, Russia*

[c] *Institute of Theoretical and Experimental Physics of the NRC "Kurchatov Institute", 117218 Moscow, Russia*

[d] *Institut Denis Poisson UMR 7013, Université de Tours, 37200 Tours, France*

[e] *RCNP, Osaka University, Osaka 567-0047, Japan*

[f] *Nuclear Science Division, Lawrence Berkeley National Laboratory, 1 Cyclotron Road, Berkeley, CA 94720, USA*

E-mail: beg.alex93@gmail.com, bornvit@gmail.com, kolucik@gmail.com, vovagoy@gmail.com, nakamura@riise.hiroshima-u.ac.jp, rnr@ihep.ru, vovchenko@lbl.gov

Lattice QCD with $N_c = 2$ and $N_f = 2$ is studied at imaginary and real quark chemical potential μ_q at temperatures above T_c. We employ various methods of analytic continuation of the net baryon number B from imaginary to real μ_q. It is demonstrated that below the Roberge-Weiss temperature the cluster expansion model provides an accurate analytic continuation of B.

The 38th International Symposium on Lattice Field Theory, LATTICE2021 26th-30th July, 2021 Zoom/Gather@Massachusetts Institute of Technology

*Speaker

PoS(LATTICE2021)493

1. Introduction

The problem of the proper theoretical understanding of the QCD phase diagram in the $\mu_B - T$ plane is still unsolved. At $\mu_q = 0$ the QCD phase diagram has been successfully studied in the framework of lattice QCD. At nonzero μ_q the lattice QCD cannot be applied directly because of the sign problem.

Two indirect approaches have been employed to compute the thermodynamical quantities at small values of parameter $\theta = \mu_q/T$. The first one employs Taylor expansion in θ around $\theta = 0$ [1–4]. Another approach uses analytic continuation from imaginary θ, where sign problem is absent, to real θ [5–13].

Here we present results of our study of two-color lattice QCD, which have received considerable attention in the literature, see, e.g. recent publications [14–18] and references therein.

The interest in studies of the two-color QCD (QC$_2$D) and other QCD-like theories stems from the following reasons. They share common properties with real QCD in some parts of their phase diagrams. Additionally they are simpler and thus allow to test numerical methods that can later be used in QCD studies. In the case considered here it is important that numerical simulations of the lattice QC$_2$D can be performed both at imaginary and at real μ_q. We use this fact to analyze the efficiency of various procedures based on the analytic-continuation method and to select the optimal one. The results of earlier studies along these lines were presented in Refs. [19–22].

2. Simulation details

The grand canonical partition function can be represented as the series[1]:

$$Z_{GC}(\theta, T, V) = \sum_{n=-\infty}^{\infty} Z_C(n, T, V)\xi^n, \tag{1}$$

where $\xi = e^{\theta}$ is the fugacity, $Z_C(n, T, V)$ are canonical partition functions, and $\theta = \dfrac{\mu_q}{T} = \theta_R + \imath\theta_I$. The inverse of the fugacity expansion has the form [23]

$$Z_C\,(n, T, V) = \int_0^{2\pi} \frac{d\theta_I}{2\pi} e^{-in\theta_I} Z_{GC}(\imath\theta_I, T, V)\ . \tag{2}$$

Z_{GC} is a periodic function of θ_I: $Z_{GC}(\theta_I, T, V) = Z_{GC}(\theta_I + 2\pi/N_c, T, V)$ [24]. As a consequence of this periodicity, $Z_C(n, T, V) \neq 0$ only for $n = N_c \cdot k$ for $k \in \mathbb{Z}$.

The details of our lattice setup are the following. We employ the tree level improved Symanzik gauge action [25] and staggered fermions with the diquark source [26],

$$S_G = \beta\left(1.667\sum_{\square}\left(1 - \frac{1}{2}\mathrm{Tr}\square\right) - 0.083\sum_{\square\square}\left(1 - \frac{1}{2}\mathrm{Tr}\square\square\right)\right), \qquad S_F = \sum_{x,y}\bar{\psi}_x D(\mu_q)_{x,y}\psi_y \tag{3}$$

where $\bar{\psi}, \psi$ are staggered fermion fields,

$$D(\mu_q)_{xy} = ma\delta_{xy} + \frac{1}{2}\sum_{\nu=1}^{4}\eta_\nu(x)\left[U_{x,\nu}\delta_{x+\hat{\nu},y}e^{\mu_q a\delta_{\nu,4}} - U^{\dagger}_{x-\hat{\nu},\nu}\delta_{x-\hat{\nu},y}e^{-\mu_q a\delta_{\nu,4}}\right], \tag{4}$$

[1]Referred to as the fugacity expansion

$\eta_1(x) = 1$, $\eta_\nu(x) = (-1)^{x_1+\ldots+x_{\nu-1}}$, $\nu = 2,3,4$. Then $Z_{GC}(\theta) = \int \mathcal{D}U e^{-S_G} (\det M)^{N_f/4}$ and the net baryon number[2]

$$B(\theta) = \frac{1}{N_c} \frac{\partial \ \ln Z_{GC}(\theta)}{\partial \theta} = \frac{N_f}{4 N_c Z_{GC}} \int \mathcal{D}U e^{-S_G} (\det M)^{N_f/4} \mathrm{tr} \left[M^{-1} \frac{\partial M}{\partial \theta} \right] , \tag{5}$$

where $M = Q^\dagger(\mu_q) Q(\mu_q) + (ma)^2$, $Q = D_{oe}$. More details can be found in [27].

We use $B(\theta)$ instead of the quark density n_q and compute it numerically in QC$_2$D at both imaginary and real quark chemical potential ($B = \dfrac{n_q V}{N_c}$). From Eqs. (1) and (5) it follows that $B(\theta)$ can be expressed in terms of the probabilities P_n that a system sampled from the grand-canonical ensemble at $\mu_q = 0$ has the baryon number n ($P_n = Z_C(nN_c)/Z_{GC}(0)$). This expression has the form[3]:

$$B(\theta) = \frac{2 \sum_{n=1}^{\infty} n P_n \sinh(n N_c \theta)}{P_0 + 2 \sum_{n=1}^{\infty} P_n \cosh(n N_c \theta)} \tag{6}$$

We perform simulations on $N_s^3 \times N_t$ lattices at $\beta = 1.7$ using the Sommer parameter $r_0 = 0.468$ fm which gives the lattice spacing $a \approx 0.062$ fm. We consider $N_s = 28$ ($L = N_s a \approx 1.74$ fm) and $N_t = 14, 12$ corresponding to $T = 227$ and 265 MeV, respectively. The pion mass $m_\pi \approx 800$ MeV. We explore the domain $T < T_{RW}$, $0 < \theta_I < \pi/2$, $0 < \mathrm{Re}\mu_q < 600$ MeV, where T_{RW} is the Roberge–Weiss temperature [24].

3. Analytic continuation from imaginary to real μ_q

Method of analytic continuation provides an extrapolation from the domain where data are available to the domain of interest and, therefore, it is based on a particular function that should be analytically continued. There are two approaches to the choice of such function: the former is based on using a partial sum of some expansion derived from first principles and model independent; the latter employs a function predicted by some model and depending on model parameters.

Let us first consider a naive analytic continuation procedure by directly utilizing the fugacity expansion of the baryon number. At $\theta = i\theta_I$ it has the form

$$-\imath B(\theta)\Big|_{\theta_R=0} \equiv \tilde{B}(\theta_I) = \sum_{n=1}^{\infty} a_n \sin(2n\theta_I) , \quad \mathrm{Re}\,\mu_q = 0 . \tag{7}$$

From the fit of the lattice data to the function

$$\tilde{B}_N(\theta_I) = \sum_{n=1}^{N} a_n \sin(2n\theta_I) , \qquad 0 \le \theta_I \le \frac{\pi}{2} \tag{8}$$

one first determines a_n and then inserts the obtained values into the truncated series

$$B_N(\theta) = \sum_{n=1}^{N} a_n \sinh(2n\theta) , \tag{9}$$

[2]In what follows we omit V and T from the arguments.

[3]Though our study is limited to the case $N_C = 2$, somewhere, we provide the expressions for arbitrary N_c.

which is assumed to describe the baryon number at real values of μ_q too.

However, a large number of independent parameters needed in this approach is poorly determined from limited statistics. Using another fit function, e.g. the one based on the formula (6) with truncated series in the right-hand side, results in multiple minima of the sum of squared residuals, in addition to the above problem. This motivates one to use model-dependent fit functions. The advantage is that only a few model parameters need to be determined in this case, which can be done using the available lattice data. Given these parameters one finds as many Fourier components a_n as needed. The disadvantage here is the use of the model assumptions.

We consider the cluster expansion model (CEM) [28] and the rational fraction model (RFM) [29], each containing two free parameters and denote the respective Fourier coefficients by $a_n^{\rm CEM}$ and $a_n^{\rm RFM}$, respectively. Here we adopt these models for QC$_2$D with two flavors.

The CEM coefficients can be represented in terms of two free parameters b and q (instead of b_1 and b_2 used in Ref. [28]), which for the two-flavor QCD read as:

$$a_n^{\rm CEM} \;=\; (-1)^{n+1}\,\frac{b\,q^{n-1}}{n}\left[1+\frac{2}{\pi^2 n^2}\right]\,,\ \text{where}\ b=\frac{\pi^2 b_1}{2+\pi^2}\quad\text{and}\quad q=-\,\frac{4\,(2+\pi^2)}{1+2\pi^2}\,\frac{b_2}{b_1}\,. \tag{10}$$

In contrast to the CEM, where the Fourier coefficients exhibit exponential scaling at large n, in the RFM they obey a power-law scaling. They can be represented in terms of two parameters d and κ by a concise formula

$$a_n^{\rm RFM} = (-1)^{n+1}\;d\;\frac{2+\pi^2 n^2}{2n^3(1+n\kappa)}\,. \tag{11}$$

Inserting expressions (10) or (11) into (8) and performing the respective fit, we extract the CEM parameters b and q or the RFM parameters d and κ from our data and thus determine all coefficients $a_n^{\rm CEM}$ or $a_n^{\rm RFM}$ making it possible to find $P_n^{\rm CEM}$ or $P_n^{\rm RFM}$.

The results of this procedure are presented in Table 1. We choose the cutoff parameter N in (8) as $N=12$ in the case of CEM and $N=20$ in the case of RFM finding that the results of the fitting procedure depend only weakly on N as it takes greater values[4].

The p values listed in Table 1 indicate that the CEM fits our data at imaginary chemical potential substantially better than the RFM. The values of $a_n^{\rm CEM}$ and $a_n^{\rm RFM}$ related to the CEM and RFM models, respectively, can be found in Ref. [30].

T, MeV	CEM				RFM			
	$p-$value	b	q	r_{bq}	$p-$value	d	κ	$r_{d\kappa}$
227	0.022	1.596(34)	0.200(46)	0.672	0.004	-0.128(56)	-1.40(17)	0.9990
265	0.063	4.209(50)	0.520(28)	0.735	0.005	6.1(4.6)	6.1(5.4)	0.9995

Table 1: Parameters b and q of the CEM and d and κ of the RFM determined from the fit to our data over the range $0\le\theta_I\le\dfrac{\pi}{2}$, the correlations r_{bq} between b and q and $r_{d\kappa}$ between d and κ are also shown.

[4]We also determine the model parameters by fitting the summed expressions (12) and (13) to the lattice data for the baryon number and for each model we obtain the parameters identical to those extracted with the truncated series.

4. Analytic continuation in CEM and RFM

Analytic expressions for the series (7) were derived in both CEM [31] and RFM [30]. We begin with the CEM expression, which is given here for $N_c = 2$ in terms of the parameters b and q:

$$B_{\rm CEM}(\theta) = \frac{b}{2q}\left\{\ln\frac{1+q\exp(2\theta)}{1+q\exp(-2\theta)} + \frac{2}{\pi^2}\left[\mathrm{Li}_3\Big(-qe^{-2\theta}\Big) - \mathrm{Li}_3\Big(-qe^{2\theta}\Big)\right]\right\}. \qquad (12)$$

Eq. (12) holds true in the limit of N_f free massless quark flavors, where $q = 1$ and $b = \dfrac{N_f N_s^3}{4N_t^3}$. As illustrated in the left panel of Fig. 1, formula (12) adequately describes our lattice data at both imaginary and real values of θ after we find the parameters b and q by fitting our data at imaginary θ. $B_{\rm CEM}(\theta)$ agrees well with the lattice data, for both temperatures and over the full range of μ_q under study: $|\mathrm{Re}\mu_q| < 800$ MeV for $T = 227$ MeV and $|\mathrm{Re}\mu_q| < 640$ MeV for $T = 265$ MeV.

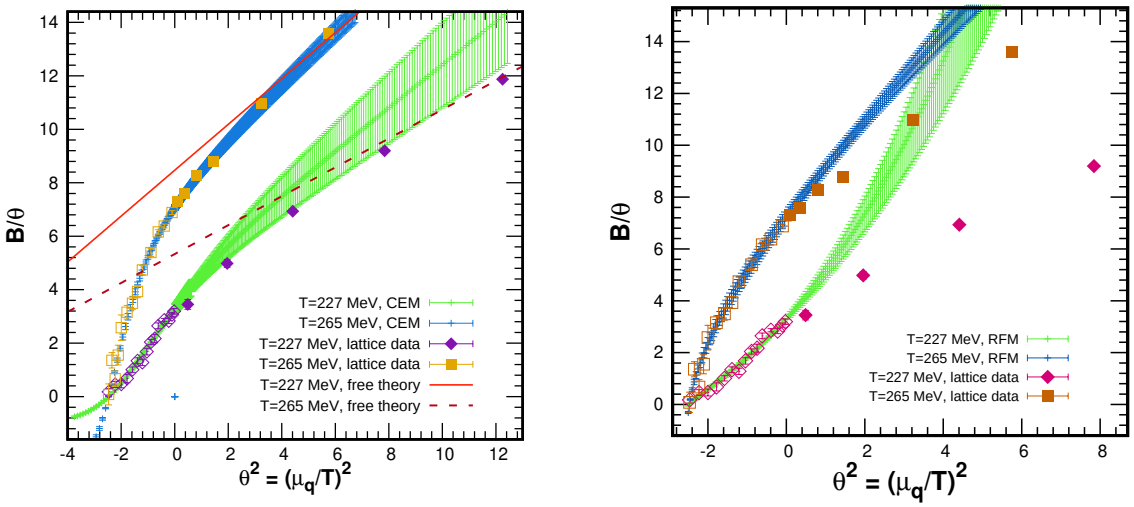

Figure 1: The lattice and free-theory results for the ratio B/θ as a function of $\theta^2 = (\mu_q/T)^2$ are compared with the results of the CEM, Eq. (12) (left panel) and RFM, Eq. (13) (right panel) at temperatures $T = 227$ MeV and 265 MeV. The baryon number in the free theory is shown only in the left panel.

The analytic expression for the series (7) in the case of RFM has the form

$$B_{\rm RFM}(\theta) = d\left\{\left(\frac{\pi^2}{2}+\kappa^2\right)\left[\theta - \left(\boldsymbol{\beta}\left(\frac{1}{\kappa}\right) - \frac{\kappa}{2}\right)\sinh\left(\frac{2\theta}{\kappa}\right) + \right.\right. \qquad (13)$$
$$\left.\left. + \frac{1}{2}\int_0^{2\theta} dt\ \tanh\frac{t}{2}\sinh\frac{2\theta - t}{\kappa}\right] + \frac{\pi^2}{6}\left(\theta + \frac{4\theta^3}{\pi^2}\right) - \kappa\int_0^{2\theta}\ln\left(2\cosh\frac{t}{2}\right)dt\right\}.$$

where $\boldsymbol{\beta}(z) = \dfrac{1}{2}\left(\psi\left(\dfrac{z+1}{2}\right) - \psi\left(\dfrac{z}{2}\right)\right)$ and $\psi(z) = \dfrac{1}{\Gamma(z)}\dfrac{d\Gamma(z)}{dz}$. The limit of free massless quarks is approached at $\kappa = 0$ and $d = \dfrac{N_f}{2\pi^2}\dfrac{N_s^3}{N_t^3}$; in Fig. 1 it is shown that the free quark limit is approached at large θ_R.

In the right panel of Fig. 1 it is clearly seen that, in contrast to the CEM, the RFM significantly deviates from the lattice data at real θ though this function fits the data equally well at imaginary θ.

To conclude, the analytic continuation of the quark density to real μ_q provided by the CEM fits lattice data much better than that provided by the RFM. This observation is similar to the conclusions of Ref. [32] regarding the description of baryon number susceptibilities in (2+1)-flavor QCD, where the CEM was also found to provide a more accurate description of the lattice data.

5. The canonical approach and limitations of the models

The probabilities P_n can be evaluated using the following procedure: (i) we find coefficients a_n either by direct fitting to Eq. (8) or using a model and (ii) we use the relation [9]

$$\frac{Z_{GC}(\imath\theta_I)}{Z_{GC}(0)} \approx \exp\left(-N_c \int_0^{\theta_I} \tilde{B}_N(x)\, dx\right) = \exp\left(N_c \sum_{n=1}^{N} \frac{a_n}{2n}\left(\cos(nN_c\theta_I) - 1\right)\right) . \qquad (14)$$

Eq. (2), and the relation $P_n = Z_C(nN_c)/Z_{GC}(0)$ to evaluate the probabilities P_n, which are then used to determine the functions providing an approximation to $B(\theta)$ at real μ_q,

$$B_N^{(Z)}(\theta) = \frac{2\sum_{n=1}^{N} nP_n \sinh(2n\theta)}{P_0 + 2\sum_{n=1}^{N} P_n \cosh(2n\theta)} . \qquad (15)$$

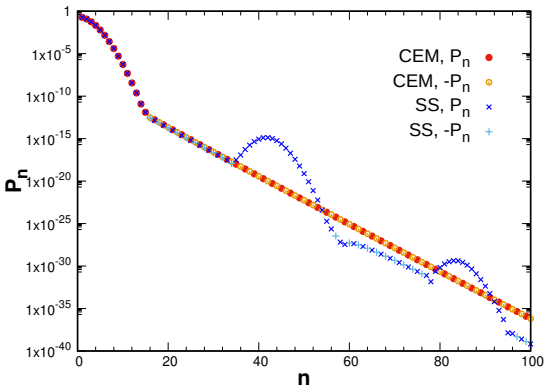

Figure 2: Dependence of P_n on n at $T = 265$ MeV. Shown are the cases when $Z_{GC}(\theta_I, T, V)$ is approximated by Eq. (12) (CEM) and by the truncated series of 41 sines (SS).

Fig. 2 illustrates the behavior of P_n in the CEM for $T = 265$ MeV obtained using the integration method. Calculations are performed in two different ways. In the first case, we use the summed baryon number from the CEM formula Eq. (12) and employ Eq. (14) to evaluate $Z_{GC}(\theta_I)$. In the second case, we approximate $B(\imath\theta_I)$ by a truncated series of sines (SS): $B_N^{\rm CEM}(\imath\theta_I) = \imath \sum_{n=1}^{N} a_n^{\rm CEM} \sin(2n\theta_I)$ with $N = 41$ and $a_n^{\rm CEM}$ given by (10). We find that the results agree with each other at $n \leq 35$. Differences occur at larger n which are attributed to the artefact of using truncated series of sines. The probabilities P_n exhibit regular behavior at $n \leq 15$, where they are all positive.

However, at $n \geq 16$ negative values of P_n are obtained which is unphysical. On one hand, this may indicate that P_n at large n are sensitive to subtle physical effects not captured by the CEM. On the other hand, the determination of P_n at large n may also be sensitive to the finite volume effects, whereas the thermodynamic limit is implicitly assumed in the CEM. For $T = 227$ MeV a qualitatively similar behavior of P_n is observed.

The expectation value of $B(\theta)$ at physical values of μ_q can be obtained not only by the analytic continuation described in the previous subsection, but also through the use of P_n via the

formulas (15) and $B^{(Z)}(\theta) = \lim_{N\to\infty} B_N^{(Z)}(\theta)$. In Fig. 3 we compare the functions

$$\frac{1}{\theta}B_N^{\rm CEM}(\theta) = \frac{1}{\theta}\sum_{n=1}^{N} a_n^{\rm CEM}\sinh(\theta) \quad \text{and} \quad \frac{1}{\theta}B_N^{(Z)}(\theta) = \frac{1}{\theta}\frac{2\sum_{n=1}^{N} nP_n\sinh(2n\theta)}{P_0 + 2\sum_{n=1}^{N} P_n\cosh(2n\theta)} \tag{16}$$

obtained in the CEM at various N. At both temperatures we see that both $B_7^{\rm CEM}(\theta)$ and $B_{13}^{\rm CEM}(\theta)$ depart from the line of lattice data dramatically when $\theta_R^2 \gtrsim 0.6$ for $T = 227$ MeV and $\theta_R^2 \gtrsim 0.12$ for $T = 265$ MeV. The point is that the series $\sum_{n=1}^{\infty} a_n^{\rm CEM}\sinh(2n\theta)$ diverges at $|\theta_R| > -\dfrac{\ln(q)}{2} \approx 0.81$ at $T = 227$ MeV and $|\theta_R| > 0.33$ at $T = 265$ MeV, as it follows from (10).

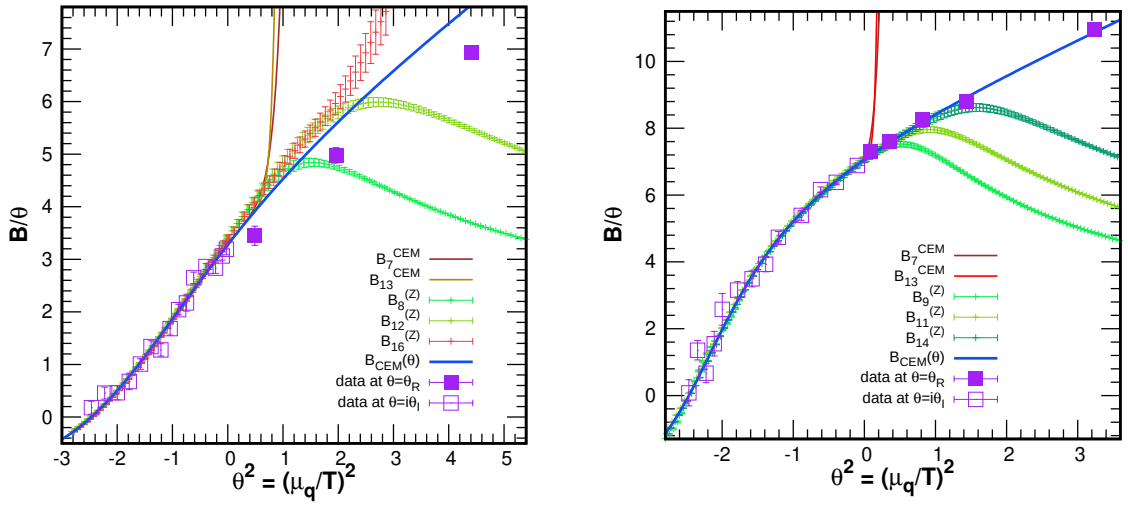

Figure 3: The functions $B_N^{\rm CEM}(\theta)$ and $B_N^{(Z)}(\theta)$ obtained in the CEM at various N are plotted versus θ^2 at $T = 227$ MeV (left panel) and $T = 265$ MeV (right panel).

As is seen in Fig. 3, the functions $B_N^{(Z)}(\theta)$ fit the lattice data well over a wide range of θ_R, which increases with N. However, there exists a maximum value of $N = N_{max}$ such that P_n at $n > N_{max}$ are not properly extracted from the data, which is indicated by alternating sign and a slow decrease of the absolute value of P_n at $n > N_{max}$ as is shown in Fig. 2. The values of N_{max} and the corresponding ranges of $\theta_R = \mu_q/T$ are as follows:

- $|\theta| < 1.7 \quad (|\mu_q| < 380$ MeV), $N_{max} = 15$ for $T = 227$ MeV,
- $|\theta| < 1.2 \quad (|\mu_q| < 320$ MeV), $N_{max} = 15$ for $T = 265$ MeV.

Since N_{max} values specified here give the upper bounds on the ranges of values of n where all P_n computed for the CEM are positive we consider the respective values of μ_q/T as the upper bounds on the domain of μ_q/T where the corrections to the CEM can be neglected.

As it follows from the previous subsection, the "direct" analytic continuation provided by the CEM agrees with lattice data in a wider range than the analytic continuation based on the grand canonical approach. However, we believe that the domain of θ_R in which the latter continuation provides a good agreement with the data expands with increasing N_{max} and if sufficiently large values of N_{max} were available on a lattice of a given size, the analytic continuation based on the

grand canonical approach would work just as well as the "direct" analytic continuation. Moreover, for a reasonable comparison of these two methods of analytic continuation one has to explain both the abrupt change of the n-dependence of P_n at $n = N_{max}$ shown in Fig. 2 and the emergence of unphysical negative values of P_n. The respective critical number N_{max} is associated with a particular quark density ρ_c, so we conclude that at $\rho < \rho_c$ both methods are valid. It should be emphasized that the method based on the grand canonical approach is model independent and stems from first principles. Therewith, the very existence of ρ_c as well as its estimates in various models is not properly understood and may be the subject of future work.

6. Conclusions

We have studied the analytic continuation of the quark density in QC_2D at $T < T_{RW}$ using various parametrizations. Their performance can be summarized as follows. We found excellent agreement with lattice data at real μ_q for the analytic continuation based on the CEM model. Good agreement was found for the grand canonical approach with the CEM at $|\mu_q| < 320 \div 390$ MeV. Poor or even bad agreement was found for RFM and the truncated Fourier series approaches.

We argue that the problem of negative probabilities P_n formulated in [30] calls for further studies.

Acknowledgments

The work was supported by the grant of the Russian Foundation for Basic Research No. 18-02-40130 mega and partially carried out within the state assignment of the Ministry of Science and Higher Education of Russia (Project No. 0657-2020-0015). This work was partially supported by Grants-in-Aid for Scientific Research (Kakenhi), No. 21K03573. For computer simulations the following resources were used: the FEFU GPU cluster Vostok-1, the Central Linux Cluster of the NRC "Kurchatov Institute" - IHEP. V.V. acknowledges the support through the Feodor Lynen program of the Alexander von Humboldt foundation, the U.S. Department of Energy, Office of Science, Office of Nuclear Physics, under contract number DE-AC02-05CH11231231, and within the framework of the Beam Energy Scan Theory (BEST) Topical Collaboration.

References

[1] R. Bellwied, S. Borsanyi, Z. Fodor, S. D. Katz, A. Pasztor, C. Ratti and K. K. Szabo, Phys. Rev. D **92** (2015) no.11, 114505 [arXiv:1507.04627 [hep-lat]].

[2] H. T. Ding, S. Mukherjee, H. Ohno, P. Petreczky and H. P. Schadler, Phys. Rev. D **92** (2015) no.7, 074043 [arXiv:1507.06637 [hep-lat]].

[3] A. Bazavov *et al.* [HotQCD], Phys. Lett. B **795** (2019), 15-21 [arXiv:1812.08235 [hep-lat]].

[4] A. Bazavov, D. Bollweg, H. T. Ding, P. Enns, *et al.* Phys. Rev. D **101** (2020) no.7, 074502 [arXiv:2001.08530 [hep-lat]].

[5] M. D'Elia and M. P. Lombardo, Phys. Rev. D **67** (2003), 014505 [arXiv:hep-lat/0209146 [hep-lat]].

[6] M. D'Elia and F. Sanfilippo, Phys. Rev. D **80** (2009), 014502 [arXiv:0904.1400 [hep-lat]].

[7] C. Bonati, P. de Forcrand, M. D'Elia, O. Philipsen and F. Sanfilippo, Phys. Rev. D **90** (2014) no.7, 074030 [arXiv:1408.5086 [hep-lat]].

[8] M. D'Elia, G. Gagliardi and F. Sanfilippo, Phys. Rev. D **95** (2017) no.9, 094503 [arXiv:1611.08285 [hep-lat]].

[9] V. G. Bornyakov, D. L. Boyda, V. A. Goy, A. V. Molochkov, A. Nakamura, A. A. Nikolaev and V. I. Zakharov, Phys. Rev. D **95** (2017) no.9, 094506, [arXiv:1611.04229 [hep-lat]].

[10] P. Alba, R. Bellwied, S. Borsanyi, Z. Fodor, J. Günther, *et al.* Phys. Rev. D **96** (2017) no.3, 034517 [arXiv:1702.01113 [hep-lat]].

[11] V. G. Bornyakov, D. L. Boyda, V. A. Goy, H. Iida, *et al.* EPJ Web Conf. **182** (2018), 02017 [arXiv:1712.02830 [hep-lat]].

[12] C. Bonati, M. D'Elia, F. Negro, F. Sanfilippo and K. Zambello, Phys. Rev. D **98** (2018) no.5, 054510 [arXiv:1805.02960 [hep-lat]].

[13] S. Borsanyi, Z. Fodor, J. N. Guenther, S. K. Katz, K. K. Szabo, A. Pasztor, I. Portillo and C. Ratti, JHEP **10** (2018), 205 [arXiv:1805.04445 [hep-lat]].

[14] V. Bornyakov, V. Braguta, A. Nikolaev and R. Rogalyov, Phys. Rev. D **102** (2020), 114511 [arXiv:2003.00232 [hep-lat]].

[15] N. Astrakhantsev, V. V. Braguta, E. M. Ilgenfritz, A. Y. Kotov and A. A. Nikolaev, Phys. Rev. D **102** (2020) no.7, 074507 [arXiv:2007.07640 [hep-lat]].

[16] P. V. Buividovich, D. Smith and L. von Smekal, Phys. Rev. D **102** (2020) no.9, 094510 [arXiv:2007.05639 [hep-lat]].

[17] K. Iida, E. Itou and T. G. Lee, PTEP **2021** (2021) no.1, 013B05 [arXiv:2008.06322 [hep-lat]].

[18] P. V. Buividovich, D. Smith and L. von Smekal, Phys. Rev. D **104** (2021) no.1, 014511 [arXiv:2012.05184 [hep-lat]].

[19] P. Giudice and A. Papa, Phys. Rev. D **69** (2004), 094509 [arXiv:hep-lat/0401024 [hep-lat]].

[20] P. Cea, L. Cosmai, M. D'Elia and A. Papa, JHEP **02** (2007), 066 [arXiv:hep-lat/0612018 [hep-lat]].

[21] P. Cea, L. Cosmai, M. D'Elia and A. Papa, Phys. Rev. D **77** (2008), 051501 [arXiv:0712.3755 [hep-lat]].

[22] P. Cea, L. Cosmai, M. D'Elia, C. Manneschi and A. Papa, Phys. Rev. D **80** (2009), 034501 [arXiv:0905.1292 [hep-lat]].

[23] A. Hasenfratz and D. Toussaint, Nucl. Phys. B **371** (1992), 539-549

[24] A. Roberge and N. Weiss, Nucl. Phys. B **275** (1986), 734-745

[25] P. Weisz, Nucl. Phys. B **212** (1983), 1-17

[26] S. Hands, J. B. Kogut, M. P. Lombardo and S. E. Morrison, Nucl. Phys. B **558** (1999), 327-346 [arXiv:hep-lat/9902034 [hep-lat]].

[27] V. Bornyakov, V. Braguta, E. M. Ilgenfritz, A. Y. Kotov, A. Molochkov and A. Nikolaev, JHEP **03**, 161 (2018) [arXiv:1711.01869 [hep-lat]].

[28] V. Vovchenko, J. Steinheimer, O. Philipsen and H. Stoecker, Phys. Rev. D **97** (2018) no.11, 114030, [arXiv:1711.01261 [hep-ph]].

[29] G. A. Almasi, B. Friman, K. Morita, P. M. Lo, and K. Redlich, Phys. Rev. D **100** (2019) no.1, 016016 [arXiv:1805.04441 [hep-ph]]

[30] A. Begun, V. G. Bornyakov, N. V. Gerasimeniuk, V. A. Goy, A. Nakamura, R. N. Rogalyov and V. Vovchenko, [arXiv:2103.07442 [hep-lat]].

[31] V. Vovchenko, J. Steinheimer, O. Philipsen, A. Pasztor, Z. Fodor, S. D. Katz and H. Stoecker, Nucl. Phys. A **982** (2019), 859-862 [arXiv:1807.06472 [hep-lat]].

[32] V. Vovchenko, J. Steinheimer, O. Philipsen and H. Stoecker, PoS **CORFU2018**, 199 (2019) [arXiv:1905.01031 [hep-ph]].